Hybrid mesh/particle meshless method for modeling geological flows with discontinuous transport properties

G. C. Bourantas[1], L. L. Lavier[2], T. Van Dam[3] and S. A. P. Bordas[1,4,5]

[1]*Faculty of Science, Technology and Communication, University of Luxembourg, Campus Kirchberg, 6, rue Richard Coudenhove-Kalergi L-1359, Luxembourg*
[2]*University of Texas, Institute for Geophysics, J. J. Pickle Research Campus Bldg. 196, 10100 Burnet Rd., Austin, TX 78758-0000, USA*
[3]*Geophysics Laboratory, Faculty of Science, Technology and Communication, University of Luxembourg Campus Kirchberg, 6, rue Richard Coudenhove-Kalergi L-1359, Luxembourg*
[4]*School of Engineering, Cardiff University, The Parade, CF24 3AA Cardiff, United Kingdom*
[5]*Intelligent Systems for Medicine Laboratory, School of Mechanical and Chemical Engineering, The University of Western Australia, 35 Stirling Highway, Crawley/Perth, WA 6009, Australia*

Abstract: In the present paper, we introduce the Finite Difference Method-Meshless Method (FDM-MM) in the context of geodynamical simulations. The proposed numerical scheme relies on the well-established FD method along with the newly developed "meshless" method and, is considered as a hybrid Eulerian/Lagrangian scheme. Mass, momentum, and energy equations are solved using an FDM method, while material properties are distributed over a set of markers (particles), which represent the spatial domain, with the solution interpolated back to the Eulerian grid. The proposed scheme is capable of solving flow equations (Stokes flow) in uniform geometries with particles, "sprinkled" in the spatial domain and is used to solve convection-diffusion problems avoiding the oscillation produced in the Eulerian approach. The resulting algebraic linear systems were solved using direct solvers. Our hybrid approach can capture sharp variations of stresses and thermal gradients in problems with a strongly variable viscosity and thermal conductivity as demonstrated through various benchmarking test cases. The present hybrid approach allows for the accurate calculation of fine thermal structures, offering local type adaptivity through the flexibility of the particle method.

Keywords: Finite Difference Method, Meshless, hybrid, Eulerian/Lagrangian.

Introduction

Solid Earth Geoscientists often must provide realistic simulations of complex nonlinear processes involving large deformation and flow of viscous material in the interior of the Earth (Gerya, 2010), such as for modelling mantle convection, subduction, continental rifting and the associated earthquakes and volcanic processes (Turcotte and Schubert, 2014; Segall, 2015). The physical phenomena involved are described by a complex set of Partial Differential Equations (PDEs), which in the majority of cases are difficult to solve

even numerically.

Modeling of large deformation in the solid Earth including elastic, viscoelastic and elastic-plastic behavior is one of the most computationally challenging tasks [1, 4]. This challenge has led to the development of multiple numerical techniques using different assumptions about the flow behavior of Earth's lithopshere (Fulsack, 1995; Braun and Sambridge, 1994; Moresi *et al*, 2003; Gerya and Yuen, 2007, Poliakov *et al*., 1993, Popov and Sobolev, 2008, Quinquis *et al*, 2011, Choi *et al*., 2008, 2013). Depending on the temperature and pressure, the lithosphere can behave as nonlinear elastic/plastic solids or as a viscoelastic fluid. In order to solve the momentum and energy conservation conditions coupled to such non-linear constitutive updates, a large contingent of the earth sciences community uses particle based Eulerian-Lagrangian methods that solves for non-linear incompressible Stokes flow (Fulsack, 1995; Moresi et al, 2003; Gerya and Yuen, 2007). In this case, the solid elastic/plastic components of the Earth' lithosphere and mantle are modeled as viscoelastic with a high viscosity and a yield stress that is dependent on pressure, such as the Drucker-Prager or Mohr-Coulomb yield criterion. In other cases, the Earth's lithosphere is modeled as anelastic solid with pressure dependent yield criterion as well (Poliakov *et al*., 1993, Popov and Sobolev, 2008, Quinquis *et al*, 2011, Choi et al., 2008, 2013). At stress magnitudes beyond the yield stress, the material follows a plastic flow law that is either associative or non associative (refs). In the elastic solid case, the quasi-static version of the momentum balance is solved using an elastic plastic constitutive update for the solid part of the lithosphere and a viscoelastic update for the viscous part of the lithosphere. Another key difference between these methods is that the incompressibility of purely viscous materials is guaranteed by the continuity equation in the Stokes flow based schemes and by near incompressible Poisson's ratio ($\nu \sim 0.5$) for the elastic solid based schemes (Babeyko *et al*., 2002; Choi *et al*., 2013).

Each numerical approach suffers from their assumptions. Stokes based approaches are Eulerian and must use additional assumptions to treat the free surface (air layer, Gerya, 2010). Moreover, the assumption of incompressibility limits the elastic treatment to the shear modulus since bulk compressibility is difficult to achieve in a viscous material (Gerya, 2010). Likewise the elastic solid treatment of the lithosphere often forces a Lagrangian frame of reference for the model grid that leads to mesh distortion and the

need for remeshing based techniques that can introduce large errors at the time of remeshing. In addition purely viscous behavior is treated as the nearly incompressible case of a Maxwell visco-elastic material. Another key aspect of simulating large lithospheric deformations are the sharp changes in material properties caused by the presence of solid/fluid boundaries and the non-linear nature of the rheology of Earth materials (Gerya and Yuen 2007; May *et al*., 2015). The viscosity of the lithosphere is non-linearly dependent on the temperature, pressure, strain rate, grain size, and other parameters derived from laboratory experiments (Burgman and Dresen, 2008). Moreover, phase changes are sometime accompanied by the formation of melt and the release of aqueous fluid in the viscous or solid matrix that result in sharply varying properties in the material (viscosity, density, material phase). These sharp material changes are extremely difficult to treat numerically. Further, fluid motion is mainly driven by the heat produced from the Earth's core and from radiogenic heat sources in the Earth's mantle. Numerical modeling of geodynamic problems typically requires the solution of the Stokes equations for creeping, highly viscous flows. A near zero Reynolds number (creeping flow/Stokes flow), represents a major challenge for solving both the momentum and energy conservation equations.

Stokes solver needs to be robust since material properties can vary many orders of magnitudes over small spatial scales and, these steep discontinuities need to be accurately resolved. A number of different numerical techniques (e.g. finite difference method (FD), finite volume (FV), finite element (FE) and spectral methods) are presently in use. Stokes flow problems have been approached in (Gerya and Yuen, 2003; Gerya *et al*., 2013) using the FDM and a combined mesh-marker approach. Therein, the flux-conservative, staggered finite-difference scheme used for solving lithospheric-scale Stokes flow has proven to be practical and reliable, in terms of the computational resources required (Gerya and Yuen, 2007; Gerya, 2010; Petersen et al., 2010), and in the quality of the numerical solution (Duretz *et al*., 2011). In (Deubelbeiss and Kaus, 2008) a number of different finite difference (FD) techniques (staggered grid, stream function and rotated staggered grid) were examined in order to evaluate their accuracies. They showed that the interpolation method used to assign viscosity parameters in the numerical grid plays an important role. In fact, the application of different interpolation methods yields

differences in accuracy of up to one order of magnitude. Regarding FEM, authors in (Moresi and Solomatov, 1995) developed a method capable of handling variations in viscosity values of up to 14 orders of magnitude and, they manage to solve 2D convection problems. Their success relies on the fact that they considered relatively smooth variations in effective viscosity field. On the other hand, sharp gradients may lead to severe divergence of the numerical solution (Tackley 2000; Albers 2000; Choblet 2005). It was shown by (Moresi *et al*., 1996) that the accuracy of the solution depends on the local (element based) variation of viscosity. In case there is a jump in material properties that occurs exactly at the element boundary, the errors in velocity and pressure are relatively independent of the total viscosity contrast. If the jump occurs inside an element, errors increased by more than two orders of magnitude (errors in velocity are one to two orders of magnitudes smaller than the errors in pressure). In fact, (Schmid, 2002) found that it was necessary to use an unstructured FEM, together with higher order (Q_2P_{-1}) shape functions (instead of the linear shape functions) to obtain accurate pressure solutions. Even if FEM would be an appropriate tool to solve a variety of geodynamics problems, it requires exact knowledge of locations of material interfaces and, there are many situations in which it would be prohibitively expensive to dynamically generate such a mesh. The most practical methods for such problems, in particular in 3D, seem to be Eulerian or arbitrary Lagrangian-Eulerian methods with quasi-structured grids as they are routinely employed in the mantle convection community. Conforming meshes seems to be quite straightforward to apply, but in many geological processes materials will undergo severe mixing and experience extremely high strains, making the use of conforming meshes to be extremely costly. On the other hand, accurate grid based advection solvers can be constructed using high order finite volume (FV) discretisations combined with flux limiters (TVD, ENO, WENO). Despite their accuracy, these methods are computationally expensive (Leveque and Li, 1997; Fedkiw *et al*. 1999; Chern and Shur, 2007; Suckale *et al*., 2010).

It has been demonstrated that FDM with marker in cell (FDM-MIC) are very efficient in solving multi-component geodynamic problems and many authors use FDM-MIC to model geodynamical processes (Gerya, 2010). Geodynamical oriented numerical methods based on FDM-MIC require the application of interpolation schemes and, if the

interpolation is carefully chosen, the accuracy of the numerical solution can be improved by almost one order of magnitude. In this paper, motivated by the absence of a robust meshless interpolating scheme in the field of geodynamics, we present a novel computational framework for geodynamical modeling, which utilizes FDM and Meshless Methods (FDM-MM). In the context of MM the simulation domain is represented by a set of nodes without any predefined information on their connectivity. Numerical simulation are not based on a mesh but connection between, but are rather based on interaction of each node with all its neighbors. The proposed scheme will provide a highly flexible framework, capable of adjusting to all the well-established numerical methods, such as FEM, FVM, spectral, and Lattice-Boltzmann. Our method has several state-of-the-art features of MM that can offer significant benefits to the geodynamical simulations.

The outline of the paper is as follows. In section 2 we begin by presenting an overview the governing flow equations, while also discussing discretization, the interpolation and solution strategies employed within the code, as well as the mesh optimization methodologies. In section 3, we demonstrate the interpolation accuracy and robustness of the proposed scheme by comparing the numerical results obtained using the Marker-In-Cell method. In section 4, we validate the accuracy and the efficiency of the proposed hybrid scheme through representative test cases (at lithospheric scales). Lastly, in section 5, we summarize the hybrid mesh-particle formulation and conclude by discussing future directions of research and other possible applications of this methodology.

2. Finite Difference-Meshless method

2.1 Governing equations

The governing equations express conservation of mass, linear momentum and energy. Flow cases considered are in the limit of low Reynolds number (creeping flow-Stokes flow) with non-linear constitutive relationships between stress and strain-rate representing shear thinning. These equations will be used to describe convective heat-transfer problems involving multiphase viscous fluids in the presence of a gravitational body force term. We assume the Boussinesq approximation for the flow cases solved,

therefore using the proposed scheme density is considered as constant in all terms except for the buoyancy force.

The conservation of mass is expressed by the continuity equation:

$$u_{i,i} = 0 \tag{1}$$

with u_i being the velocity components. Conservation of linear momentum is expressed by the Stokes equations of creeping flow, where the inertial terms of the Navier-Stokes equations are dropped. Stokes equations are written as:

$$\tau_{ij,j} - p_{,i} = f_i \tag{2}$$

along with boundary conditions

$$u_i = g_i \quad on\ \partial\Omega_D \tag{3}$$

$$\sigma_{ij} n_j = h_i \quad on\ \partial\Omega_N \tag{4}$$

where u_i corresponds to velocity components (i=x,y), τ_{ij} is the deviatoric stress tensor defined as τ_{ij}=2$\eta\varepsilon_{ij}$ with η being the viscosity of the material, p is the dynamic pressure, n_i is the unit outward normal vector to the boundary of the domain $\partial\Omega = \partial\Omega_D \cup \partial\Omega_N$, where $\partial\Omega_D$ and $\partial\Omega_N$ correspond to Dirichlet and Neumann boundary conditions, respectively and g_i, h_i are given functions.

The right hand side in Eq. (2) represents the body forces which can be the, in the majority of the cases, a function of temperature (T), pressure (p), chemical components (C) and strain-rate. The strain rate tensor ε_{ij} used in the computation of the deviatoric stress tensor τ_{ij} is defined as

$$\varepsilon_{ij} = \frac{1}{2}\left(u_{i,j} + u_{j,i}\right) \tag{5}$$

Energy (temperature) equation is solved using a Lagrangian framework, with the governing equations written as

$$\rho C_p\left(T_{,t} + u_i T_{,i}\right) = q_{i,i} + H_r + H_a + H_s \tag{6a}$$

$$q_i = k(T,P)T_{,i} \quad (6b)$$

$$H_r = ct \quad (6c)$$

$$H_a = aTu_iP_{,i} \quad (6d)$$

$$H_s = \sigma_{xx}\varepsilon_{xx} + \sigma_{zz}\varepsilon_{zz} + 2\sigma_{xz}\varepsilon_{xz} \quad (6e)$$

2.2 Computational Strategy

Our approach is in many ways similar to that described in (Gerya and Yuen, 2003). The governing equations are solved using a hybrid Eulerian/Lagrangain method, velocity components and pressure are computed in the Eulerian framework while, physical and material properties advected in the Lagrangian. In detail, Stokes equations are solved using a stress-conservative (eliminates spurious pressure oscillations across adjacent cells), fully staggered (orthogonal, block-structured) finite-difference (FD) grid, combined with a particle/marker based method. In the context of the hybrid mesh/particle method, scalar properties (density, viscosity, thermal conductivity, thermal diffusivity, temperature etc), assigned to a set of markers distributed, randomly or uniformly, along the spatial domain, are first interpolated from particles to grid points so that the Stokes flow equations can be solved. Following, the computed velocity field and pressure are interpolated back to the markers in order to advect them through space and time.

The efficiency and accuracy of this method strongly depends on the interpolating scheme used (Deubelbeiss and Kaus, 2008). Geodynamic processes strongly depend on a number of physical characteristics, which are often non-linear, distributed heterogeneously and are, therefore, challenging from a numerical modeling perspective. In fact, the most important property is the rheology that governs the deformation of Earth materials, especially the high strain heterogeneities in the material. Numerical methods applied and numerical codes developed, must be able to advect material properties, track with accuracy the interfaces of the various materials and compute the values of material properties variables (temperature, stress velocity, grain size) throughout the model.

Particle based methods can accurately and efficiently deal with all these issues.

The scheme proposed here relies on a meshless interpolation method. In the meshless literature a number of interpolating/approximating methods exist (Liu, 2002; Atluri, 2004; Fasshauer, 2007). Among them, the most widely used are the Moving Least Squares (MLS), Radial Basis Functions (RBF) and Smoothed Particle Hydrodynamics (SPH) (Lucy, 1997; Gingold and Monaghan, 1982). Each one of these interpolation methods can be used for assigning values to the grid nodes from the markers. Although, driven by the physical concept of the proposed hybrid scheme we are using SPH kernels, which are originally used for particles. High order kernels are used able to resolve accurately the steep discontinuities in the material properties.

In the context of kernel-based interpolation, any function $A(\boldsymbol{r})$ is approximated by an integral interpolation:

$$A(\boldsymbol{r}) = \int A(\boldsymbol{r}) W(\boldsymbol{r} - \boldsymbol{r}', h) d\boldsymbol{r}' \tag{7}$$

where $W(\boldsymbol{r} - \boldsymbol{r}')$ is the weighting function or kernel and h is the smoothing length. The above formulation is valid within the continuum, the discrete one can be written as:

$$A(\boldsymbol{r}) = \sum_i A_i W(\boldsymbol{r} - \boldsymbol{r}_i, h) \tag{8}$$

with the summation being over particles (i) located in the support domain of the kernel function. The accuracy of the interpolation scheme depends on the choice of the weighting function, which is a normalized function, positively defined, with compact support and monotonically decreasing with increasing distance from the center particle. The following kernels are widely used in the context of meshless methods

(1) *Gaussian*:

$$W(r, h) = a_D e^{-q^2} \tag{9}$$

(2) *Quadratic*:

$$W(r, h) = a_D \left(\frac{3}{16} q^2 - \frac{3}{4} q + \frac{3}{4} \right), \quad 0 \le q \le 2 \tag{10}$$

(3) *Cubic spline*:

$$W(r,h) = a_D \begin{cases} 1 - \frac{3}{2}q^2 + \frac{3}{4}q^3, & 0 \le q \le 1 \\ \frac{1}{4}(2-q)^3, & 1 \le q \le 2 \\ 0, & q \ge 2 \end{cases} \tag{11}$$

(4) *Quintic*

$$W(r,h) = a_D \left(1 - \frac{q}{2}\right)^4 (2q+1), \quad 0 \le q \le 2 \tag{12}$$

High-order accurate interpolation schemes are not producing unwanted spurious oscillations near the sharp discontinuities, in contrast to the fluctuations reported in (Fornberg, 1995) when high order scheme are used, stressing out the stability of the proposed schemes. An important issue regarding the applicability of the meshless scheme is related to the computational cost involved. The computational cost for the neighboring nodes definition was the bottleneck in the interpolation procedure. In practice, naïve implementation of shape function calculation takes into account long-range interactions occurring in the entire spatial domain, imposes a computational cost of $O(N^2)$, which is prohibitive for real-time simulations. Analyzing meshless methods reveals important locality properties. Taking advantage of these local properties existing methodologies provide approximate solutions in much lower complexity bounds equal to $O(N\log N)$ and $O(N)$ using fast N-body solvers such as the Barnes-Hut algorithm (Barnes and Hut, 1986) and Fast Multipole Methods (Greengard and Gropp, 1990). Additionally, interactions that only involve local neighborhood can efficiently be computed in $O(N)$ time using fast neighbor lists, such as cell lists (Hockney and Eastwood, 1988) or Verlet lists (Verlet, 1967). In the present study computational efficiency is achieved by observing that each node in the grid interacts only with local neighbors in a small subdomain of the original grid, thus avoiding computations from each point to every other point that raise the cost to $O(N^2)$. The hashing pre-processing step introduces a computational overhead, which is linearly proportional to the number of nodes ($O(N)$ complexity). In total, preprocessing and mapping steps are performed linearly in time leading to a significant performance

gain as the problem dimensionality increases. In fact, meshless methods, due to their regular computational structure and fine granularity, are suitable for parallelization.

The algorithmic steps for the proposed FDM-MM scheme are:

1. Define the spatial domain and create a set of markers. Assign material and physical properties to the markers
2. Calculate effective material properties values on the grid nodes by interpolating values from the markers
3. Solve the governing equations (Stokes flow) by using a direct method.
4. Calculate deviatoric shear stress and adiabatic heating terms
5. Calculate the total time derivative DT/Dt on the Eulerian mesh by using an explicit method.
6. Define an optimal time step based on the CFL criterion (markers displacement step is related to the time step).
7. Solve the non-linear energy equation implicitly (Gauss elimination method).
8. Interpolate temperature changes back to the markers using the meshless kernel, assigning updated temperature values to the markers.
9. Advect markers through the spatial domain by using a Runge-Kutta scheme (fourth order in space and first order in time). Computations are held based on the calculated velocity field on the mesh nodes.
10. Calculate scalar physical properties (viscosity, density, heat capacity, thermal conductivity, etc) on the markers. Interpolate temperature and scalar properties from markers to mesh nodes.
11. Return back to Step 1.

3. Verification of the approximation scheme

In order to test and quantify the interpolation properties of the proposed meshless scheme, three benchmark problems with analytical solutions were employed. The benchmark problems deal with variable viscosity, incompressible steady state flow problems. They are considered as representative problems in the framework of

geodynamics, since the applied viscosity variations (considered as both sharp and smooth) are analogous to geodynamic problems.

For all the test cases considered, we are interested in the interpolation aspects of the meshless kernel. We are mainly concerned about its ability to capture the steep discontinuities of the material properties, since the accuracy and efficiency of the finite difference solver is depicted elsewhere (Gerya *et al*., 2103).

3.1 SolKz analytical solution

The first problem considered is the SolKz benchmark problem (Gerya *et al*., 2103), which is characterized by an exponential variation in viscosity from bottom to top of the spatial domain, defined as $\Omega = [0,1]\times[0,1]$. In all boundaries free slip boundary conditions were applied. Fluid flow is driven by sinusoidal force given by $F = \left(0, -sin(1.6\pi y)cos(3\pi x)\right)^T$, which is imposed practically by setting gravity acceleration components g_x and g_y as g_x=0 and g_y=1, while setting the density field as $\rho(x,y) = sin(2y)cos(3\pi x)$. The viscosity field varies exponentially in the y direction according to $\eta(y) = e^{2B(1-y)}$, with the parameter B=6.9.

For the simulations conducted, we considered uniform semi-staggered grid configurations with increasingly denser spatial resolution, starting by 51×51 up to 201×201 nodes. The successive grids provided a grid independent solution. The numerical results obtained using the meshless scheme were compared against the MIC method (Gerya, 2010) and they were in excellent agreement. Fig. 1 shows the velocity components u_x, u_y in the x- and y- direction, respectively, along with pressure plot, with the numerical results obtained using a grid of 201×201 nodes and 1 million markers. The SolKz benchmark problem was solved using the FDM-MIC method and numerical results obtained were compared against those obtained using the FDM-MM scheme. In Fig. 2 the error distribution (discrete maximum absolute error) for a 201×201 grid resolution is shown.

3.2 SolCx analytical solution

Next, we considered the case of the SolCx analytical solution problem (Gerya *et al*., 2103), which exhibits a discontinuity in the viscosity in the *x*- direction. The spatial domain is defined as $\Omega = [0,1]\times[0,1]$. In all boundaries free slip boundary conditions were applied. Fluid flow is driven by sinusoidal force given by $F = \left(0, -sin(\pi y)cos(\pi x)\right)^T$, which is imposed practically by setting gravity acceleration components g_x and g_y as g_x=0 and g_y=1 and setting the density field as $\rho(x,y) = sin(2y)cos(3\pi x)$. The viscosity field is defined as

$$\eta(x,y) = \begin{cases} 1, & 0 \le x \le 0.5 \\ 10^6, & 0.5 < x \le 1 \end{cases} \tag{13}$$

We considered uniform semi-staggered grid configurations with increasingly denser spatial resolution, starting by 51×51 up to 201×201 nodes. The successive grids provided a grid independent solution. The numerical results obtained using the meshless scheme were compared against the MIC method and they were in excellent agreement. Fig. 3 shows the u_x, u_y and pressure plots using a grid of 201×201 nodes and 1 million markers. The SolCx benchmark problem was solved using the FDM-MIC method and numerical results obtained were compared against those obtained using the FDM-MM scheme. In Fig. 4 the error distribution (discrete maximum absolute error) for a 201×201 grid resolution is shown.

3.3 Viscous inclusion- SolVI test

The final verification problem considered is the viscous inclusion test problem (Gerya *et al*., 2103, Schmid, 2002], which deals with a homogeneous circular inclusion embedded in a homogeneous matrix of different. The spatial domain is given by $\Omega = [-1,1]\times[-1,1]$ with the circular inclusion located at (0,0) having radius of R_{inc}=0.5. The viscosity is assigned $\eta(x,y) = 1$ in the background and $\eta(x,y) = 10^3$ in the inclusion. Pure shear background strain rate boundary conditions are considered, with the analytical solution of the velocity of (Schmid and Podladchikov, 2003) is implemented at all four boundaries. The applied velocity boundary conditions are compressive in horizontal and extensional in vertical directions.

We considered uniform semi-staggered grid configurations with increasingly denser spatial resolution, starting by 51×51 up to 201×201 nodes. The successive grids provided a grid independent solution. In (Schmid and Podladchikov, 2003) a 2D analytical solution is derived for the prescribed geometry. Pressure is defined throughout the entire domain and for the previously described pure shear boundary conditions, is zero inside the strong clast and obtains its highest and lowest values directly at the clast-matrix interface. Pressure is used to evaluate the accuracy of the proposed numerical schemes and consequently the meshless interpolation method. Fig. 5 shows the numerically computed pressure distribution using the FDM-MIC and FDM-MM, respectively along with the error distribution (discrete maximum relative error) that shows a relative error of 16%. Computations were held using a grid of 201×201 nodes and 1 million markers. It can be seen that the highest errors occur close to the material interface (at the boundary between clast and matrix).

4. Numerical examples

To study accuracy, efficiency, and error convergence of the proposed scheme we considered flow problem (Stokes flow) having spatially varying viscosity and density (both having steep gradients). The robustness and the accuracy of the proposed scheme heavily relies on the interpolation capabilities of the kernel used, in particular, on its ability to accurately resolve the steep gradients that are present in the material properties.

4.1 Falling block

We consider the case of a rigid body sinking in a surrounding medium with low viscosity (Gerya, 2010). The velocity of the object depends on the viscosity of the surrounding medium. The block has dimensions 100×100 Km while the surrounding medium is of 500×500 Km. Free-slip boundary conditions are applied in all boundaries. For the material properties considered, the density and viscosity of the block are 3,300 (Kg/m^3) and $\eta=10^{21}$-10^{27}(Pa s), while for the surrounding material 3,200 (Kg/m^3) and $\eta=10^{21}$ (Pa s), respectively.

For the simulations conducted we used staggered grids with increasing spatial resolution, starting by 51×51 up to 201×201, and number of markers (up to 16 millions) used to represent the spatial domain and material properties. The numerical results presented were computed using a uniform staggered grid of 201×201 nodes and a total of 4 million markers. The time step is computed such that the CFL conditions were fulfilled. Fig. 6 shows the density values computed on the Eulerian mesh at different viscosity contrast between the block and the surrounding medium, while Fig. 7 shows the orientation of the markers in the spatial domain. The numerical results obtained using the FDM-MM scheme were compared against those using FDM-MIC (Gerya, 2010) and they were in an excellent agreement. A way of monitoring the accuracy of MM interpolating scheme is by comparing the time step computed using MM with the time step computed using MIC. This can be proved to be a concise way of comparison since time step calculation is directly related to the maximum velocity computed by solving the flow equations and is correlated with the CFL conditions of the markers. Thus, by comparing the time steps computed by the two interpolating methods we can deduce on the accuracy. For our computations using the exact same specifications (Eulerian grid and number of particles) the relative maximum absolute error of the time steps was of 10^{-4}.

4.2 Falling block with temperature

Next, we consider the case of a rigid body sinking in a surrounding medium with a viscosity and thermal conductivity different than that of the sinking body taking into account the exchange of energy, thus temperature variations. As in the previous example, the block has dimensions 100×100 Km with the surrounding medium being 500×500 Km. We prescribe a different temperature and thermal conductivity to the surrounding medium (T=1000 K, k=1 W/m/K) and for the sinking block (T=1300 K, k=10 W/m/K). For the simulations conducted we considered insulating boundary conditions on all boundaries for the temperature field and free-slip velocity boundary conditions. We considered radiogenic (10^{-6} W/m^3 and 10^{-7} W/m^3 for the block and surrounding material, respectively), shear, and adiabatic heating terms in the temperature equation. The density of the surrounding medium was set to 3,200 Kg while the falling block has density of

3,330 Kg. For the viscosity we considered 10^{21} (Pa s) and 10^{22} (Pa s) for the surrounding medium and the falling block, respectively.

For the simulations conducted we used staggered grids with increasing spatial resolution, starting by 51×51 up to 201×201, and number of markers (up to 16 millions) used to represent the spatial domain and material properties. The numerical results presented were computed using a uniform staggered grid of 201×201 nodes and a total of 1 million markers. Regarding the time step used, we restricted the time step by limiting the maximal temperature changes to 20 K per time step (Gerya, 2010), meaning that if changes are bigger than 20 K, then time step is proportionally repeated and the numerical solution is repeated for a second time (the computational cost is not considerably increased since the numerical solution of the temperature equation is computationally inexpensive compared to the momentum and continuity equations). Fig. 8 shows the temperature values computed on the Eulerian mesh at different viscosity contrast between the block and the surrounding medium. The numerical results obtained using the FDM-MM scheme were compared against those using FDM-MIC (Gerya, 2010)and they were in an excellent agreement. For the computations conducted using the same specifications (Eulerian grid and number of particles) the relative maximum absolute error of the time steps was of 10^{-4}.

4.3 Thermal convection with large viscosity contrast conductivity

Finally, we consider the case of thermal convection with temperature dependent viscosity, density and thermal conductivity, which is considered as a challenging test case in geodynamics (Moresi and Salamatov, 1995). Simulations were held in a square domain with dimensions of 500 Km, represented by an Eulerian uniform grid of 201 nodes in each direction. The material properties were assigned on a set of markers (one million markers in total), uniformly distributed all over the domain. The boundary conditions applied, correspond to free-slip along all boundaries considering momentum equations and, specified temperature on the top (T_0=273 K) and at the bottom (T_1=2,773 K) along with adiabatic ($T_{,x} = 0$) at the vertical walls for energy conservation. The variable,

temperature-dependent viscosity considered for the simulations is given according to the Frank-Kamnetzky approximation (Moresi and Salamatov, 1995; Albers, 2000)

$$\eta = \eta_0 e^{-ln\left(\frac{\eta_0}{\eta_1}\right)\left(\frac{T-T_0}{T_1-T_0}\right)} \tag{14}$$

where η_0 and η_1 are the maximal and minimal values of viscosity (η_0.=10^{21} and the ratio of η_0/η_1 ranges from 10^2 to 10^7). The temperature dependent density is given by

$$\rho = \rho_0 e^{1-2.5*10^{-5}(T-T_0)} \tag{15}$$

where $\rho_0 = 4000\, kg/m^3$, while thermal conductivity is defined by the following equation (Hofmeister, 1999)

$$k = 0.73 + \frac{1293}{T+77} \tag{16}$$

For the simulations conducted we do not account for the effects of shear and adiabatic heating. We restricted the time step by limiting the maximal temperature changes to 10 K per time step (Gerya, 2010). Fig. 9 shows the isotherms at different time steps considering various ratios of viscosity. The numerical results of FDM-MM were compared against the FDM/MIC and the numerical results were again in excellent agreement.

5. Conclusions

In this paper, we developed a finite difference/meshless method (FDM-MM) for numerically solving the incompressible Stokes flow equations frequently used in geodynamics applications. Its novelty relies on the meshless interpolation scheme combined with the FD method, which proved to be accurate and efficient, having all the features needed in a state-of-the-art geodynamics oriented method. The implementation of the meshless scheme is quite easy and straightforward. The advantages is that is local and fast to compute, especially when sophisticated nearest neighboring techniques (cell-lists, Verlet lists) are used. The computational cost for the interpolation is eliminated and

the computational burden is mostly related to the numerical solution of the Stokes flow. The FD method utilizes fully staggered grids and by applying direct matrix inversion technique solves accurately both the conservation of momentum and energy equations in 2D and 3D. Furthermore, a combination of explicit and implicit methods made possible the efficient solution also of energy equations using particle based methods.

Further development of the method relies in a meshless oriented solver. This solver will be based on a generalization of the classical Finite Difference Method through the Radial Basis Function Finite Difference Method (RBF-FD). Additionally, the meshless interpolation method will be extended to use different interpolating schemes, mostly in particle methods. The applicability of the method will be evaluated in a high-computing framework since the meshless scheme is inherently parallelized. The method will be extended and tested to more demanding geodynamics problems by adding viscoelasticity and plasticity. The same marker technique can also be applied in thermal-chemical convection, the viscoelastic stress-transfer problems. The work set out here lays the foundation for future in these aforementioned areas.

References

Gerya, T.V., 2010. Introduction to Numerical Geodynamic Modelling, 358 pp. Cambridge University Press, New York.

Turcotte, D.L., Schubert G., 2014. Geodynamics, 3rd Ed. Cambridge University Press, 636 pp .

Segall P., 2015. Earthquake and Volcano Deformation, Princeton University Press, 456 pp.

Fullsack, P., 1995. An arbitrary Lagrangian-Eulerian formulation for creeping flows and its application in tectonic models. Geophys. J. Int. 120, 1-23.

Braun, J., Sambridge, M., 1994. Dynamical Lagrangian Remeshing (DLR): A new algorithm for solving large strain deformation problems and its application to fault-propagation folding. Earth Planet Sci. Lett. 124 (1-4), 211-220, doi:10.1016/0012-821X(94)00093-X.

Moresi, L. N., Dufour, F., Mühlhaus, H. -B., 2003. A Lagrangian integration point finite element method for large deformation modeling of viscoelastic geomaterials. J. Comput. Phys. 184(2), 476-497, doi:10.1016/S0021-9991(02)00031-1.

Gerya, T., Yuen, D., 2007. Robust characteristics method for modelling multiphase visco-elasto-plastic thermo-mechanical problems. Phys. Earth Planet. Inter. 163, 83-105, doi:10.1016/j.pepi.2007.04.015.

Poliakov, A. N. B., Cundall, P. A., Podladchikov, Y. Y. Lyakhovsky, V. A., 1993. An explicit inertial method for the simulation of viscoelastic flow: An evaluation of elastic effects on diapiric flow in two- and three-layers models, inFlow and Creep in the Solar Systems: Observations, Modeling and Theory, edited by D. B. Stone, and S. K. Runcorn, pp. 175-195, Kluwer Academic Publishers, Dordrecht.

Popov, A., Sobolev, S., 2008. SLIM3D: A tool for three-dimensional thermomechanical modeling of lithospheric deformation with elasto-visco-plastic rheology. Phys. Earth Planet. Inter. 171, 55-75, doi:10.1016/j.pepi.2008.03.007.

Quinquis, M.E.T., Buiter, S.J.H., Ellis, S., 2011. The role of boundary conditions in numerical models of subduction zone dynamics. Tectonophysics 497, 57-70, doi:10.1016/j.tecto.2010.11.001.

Choi, E., Lavier, L., Gurnis, M., 2008. Thermomechanics of mid-ocean ridge segmentation. Phys. Earth Planet. Inter. 171, 374-386, doi:10.1016/j.pepi.2008.08.010.

Choi E., Tan, E., Lavier, L. L., Calo, V. M., 2013. DynEarthSol2D: An efficient unstructured finite element method to study long-term tectonic deformation. J. Geophys. Res. Solid Earth. 118, 2429-2444, doi:10.1002/jgrb.50148.

Babeyko, A.Y., Sobolev, S.V., Trumbull, R.B., Oncken, O., Lavier, L.L., 2002. Numerical models of crustal scale convection and partial melting beneath the Altiplano-Puna plateau. Earth Planet. Sci. Lett. 199, 373-388, doi:10.1016/S0012-821X(02)00597-6.

May, D.A., Brown, J., Le Pourhiet, L., 2015. A scalable, matrix-free multigrid preconditioner for finite element discretizations of heterogeneous Stokes flow. Computer Methods in Applied Mechanics and Engineering 290, 496-523.

Bürgmann, R., Dresen, G., 2008. Rheology of the lower crust and upper mantle: Evidence from rock mechanics, geodesy, and field observations. Annual Review of Earth and Planetary Sciences. 36, 531-567.

Gerya, T.V., Yuen, D.A., 2003. Characteristics-based marker-in-cell method with conservative finite-differences schemes for modeling geological flows with strongly variable transport properties. Physics of the Earth and Planetary Interiors 140, 293-318.

Gerya, T.V., May, D.A., Duretz, T., 2013. An adaptive staggered grid finite difference method for modeling geodynamic Stokes flows with strongly variable viscosity. Geochemistry, Geophysics, Geosystems 14 (4), 1200-1225.

Petersen, K.D., Nielsen, S.B., Clausen, O. R., Stephenson, R., Gerya, T.V., 2010. Small-scale mantle convection produces stratigraphic sequences in sedimentary basins. Science 329, 827-830, doi:10.1126/science.1190115.

Duretz, T., May, D.A., Gerya, T.V., Tackley, P.J., 2011. Discretization errors and free surface stabilization in the finite difference and marker-in-cell method for applied geodynamics: A numerical study. Geochem. Geophys. Geosyst. 12,, doi:10.1029/2011GC003567.

Deubelbeiss Y., Kaus B.J.P., 2008. Comparison of Eulerian and Lagrangian numerical techniques for the Stokes equations in the presence of strongly varying viscosity. Physics of the Earth and Planetary Interiors 171, 92-111.

Moresi L., Solomatov, V., 1995. Numerical investigations of 2D convection in a fluid with extremely large viscosity variations. Physics of Fluids 7, 2154-2162.

Tackley P., 2000. Self-consistent generation of tectonic plates in time-dependent, three-dimensional mantle convection simulations. Part 1. Pseudoplastic yielding. Geochem. Geophys. Geosyst. 01 (23)

Albers M., 2000. A local mesh refinement multigrid method for 3D convection problems with strongly variable viscosity. Journal of Compuational Physics 160 (1), 126-150.

Choblet G., 2005. Modelling thermal convection with large viscosity gradients in one block of the “cubed sphere”. Journal of Computational Physics 205 (1), 269-291.

Moresi L., Zhong S., Gurnis M., 1996. The accuracy of finite element solutions of Stokes’s flow with strongly varying viscosity. Physics of the Earth and Planetary Interiors 97 (1-4), 83-94.

Schmid, D.W., 2002. Finite and Infinite Heterogeneities Under Pure and Simple Shear. PhD. Swiss Federal Institute of Technology.

Leveque, R.J., Li Z., 1997. Immersed interface methods for Stokes flow with elastic boundaries or surface tension. SIAM J. Sci. Comput. 18(3), 709-735.

Fedkiw, R.P., Aslam, T., Merriman, B., Osher, S., 1999. A non-oscillatory Eulerian approach to interfaces in multimaterial flows (the ghost fluid method). J. Comput. Phys. 152 (2), 457-492.

Chern, I.L., Shur, Y.C., 2007. A coupling interface method for elliptic interface problems. J. Comput. Phys. 225(2), 2138-2174.

Suckale, J., Nave, J.-C., Hager, B.H., 2010. It takes three to tango: 1. Simulating buoyancy-driven flow in the presence of large viscosity contrasts. J. Geophys. Res. 115, B07409.

Liu, G.R., 2002. Mesh Free Methods, Moving beyond the Finite Elements Method, CRC Press.

Atluri, S.N., 2004. The Mesheless Method (MLPG) for Domain & BIE Discretizations, Tech Science Press.

Fasshauer, G., 2007. Meshfree approximation methods with MATLAB. Singapore: World Scientific.

Lucy, L.B., 1977. A numerical approach to the testing the fission hypothesis. Astronomical Journal 82, 1013-1024.

Gingold, R.A., Monaghan, J.J., 1982. Kernel estimates as a basis for general particle methods in hydrodynamics. Journal of Computational Physics 46, 429-453.

Fornberg, B., 1995. A Practical Guide to Pseudospectral Methods. Cambridge University Press, Cambridge, pp 231.

Barnes, J., Hut P., 1986. A hierarchical O(NlogN) force-calculation algorithm. Nature 324, 446-449.

Greengard, L., Gropp W.D., 1990. A parallel version of the fast multipole method. Computers & Mathematics with Applications 20, 63-71.

Hockney, R.W., Eastwood, J.W., 1988. Computer Simulation using Particles, Institute of Physics Publishing.

Verlet, L., 1967. Computer experiments on classical fluids. I. Thermodynamical properties of Lennard-Jones molecules. Phys. Rev. 159 (1), 98-103.

Gerya, T.V., May, D.A., Duretz, T., 2013. An adaptive staggered grid finite difference method for modeling geodynamic Stokes flows with strongly variable viscosity. Geochemistry, Geophysics, Geosystems. 14, 1200-1225, doi:10.1002/ggge.20078.

Schmid, D.W., Podladchikov, Y.Y., 2003. Analytical solutions for deformable elliptical inclusions in general shear. Geophys. J. Int. 155, 269-288.

Hofmeister, A.M., 1999. Mantle values of thermal conductivity and the geotherm from phonon lifetimes. Science 283,1699-1706.

Figure captions

Fig. 1. Contour plots of **(a)** *u*- velocity **(b)** *v*- velocity and **(c)** pressure the analytical solution SolKz.

Fig. 2. Spatial distribution of absolute error for **(a)** *u*- velocity **(b)** *v*- velocity and **(c)** pressure for the analytical solution SolKz.

Fig. 3. Contour plots of **(a)** *u*- velocity **(b)** *v*- velocity and **(c)** pressure the analytical solution SolCx.

Fig. 4. Spatial distribution of absolute error for **(a)** *u*- velocity **(b)** *v*- velocity and **(c)** pressure for the analytical solution SolCx.

Fig. 5. 2D pressure fields using a viscosity contrast of $\frac{\mu_{inclusion}}{\mu_{matrix}} = 1000$ and a resolution of 201×201 for **(a)** FDM-MIC and **(b)** FDM-MM and **(c)** Spatial distribution of absolute error for the analytical solution SolVI.

Fig. 6. Density distribution for the sinking of a rectangular block at different viscosity contrast between the block and the surrounding soft medium.

Fig. 7. Orientation of the markers for the sinking of a rectangular block at different viscosity contrast between the block and the surrounding soft medium.

Fig. 8. Temperature distribution for the sinking of a rectangular block at different viscosity contrast between the block and the surrounding soft medium.

Fig. 9. Temperature contours for the non-linear convection problem with different ratios of viscosity **(a)** $\eta_0/\eta_1 = 10^2$ and **(b)** $\eta_0/\eta_1 = 10^4$.

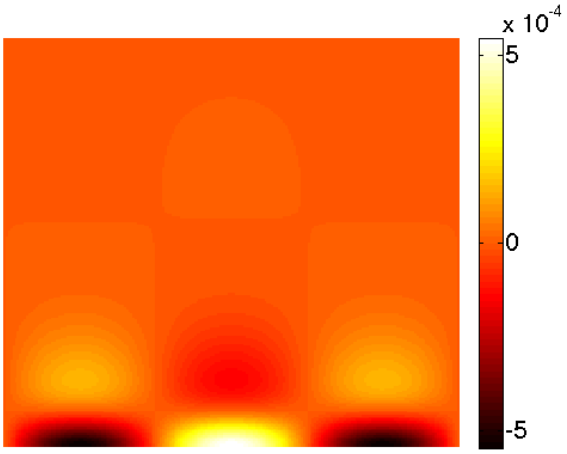

(a)

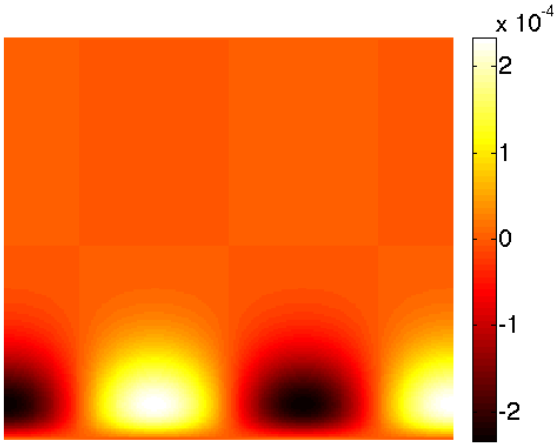

(b)

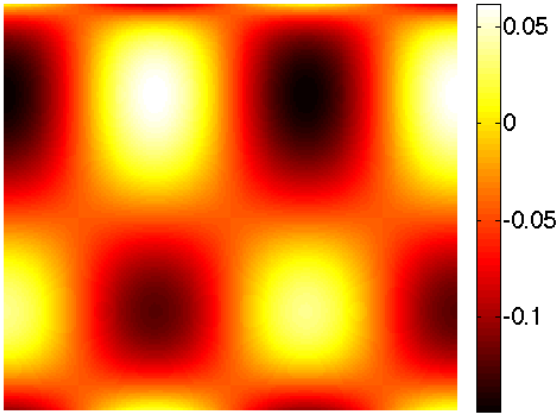

(c)

Fig. 1

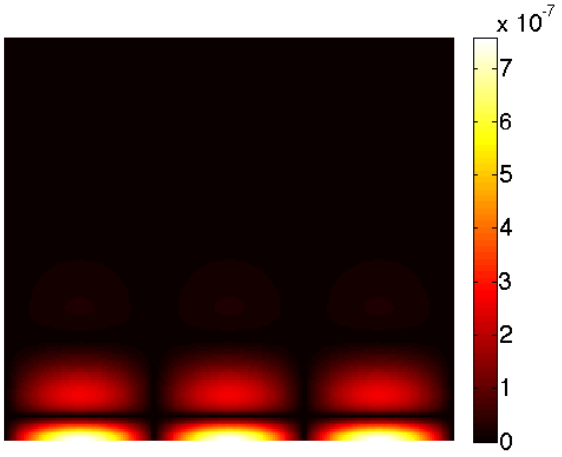

(a)

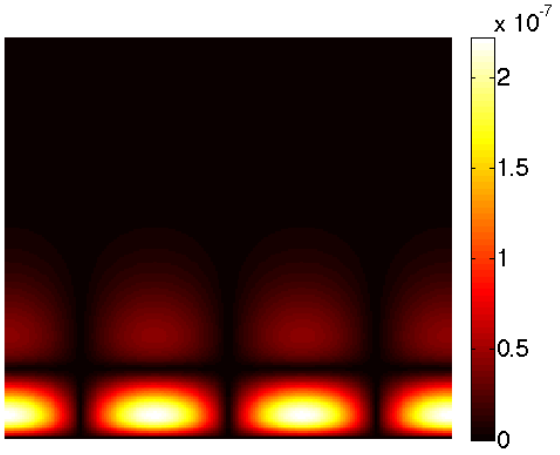

(b)

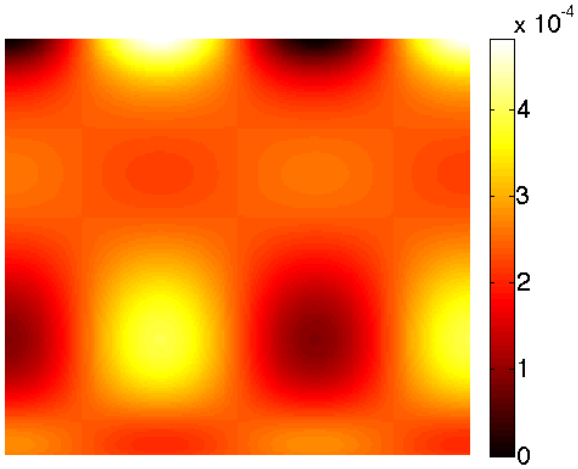

(c)

Fig. 2

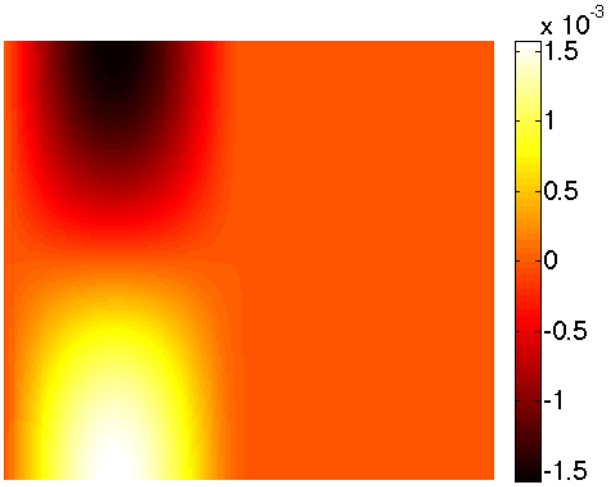

(a)

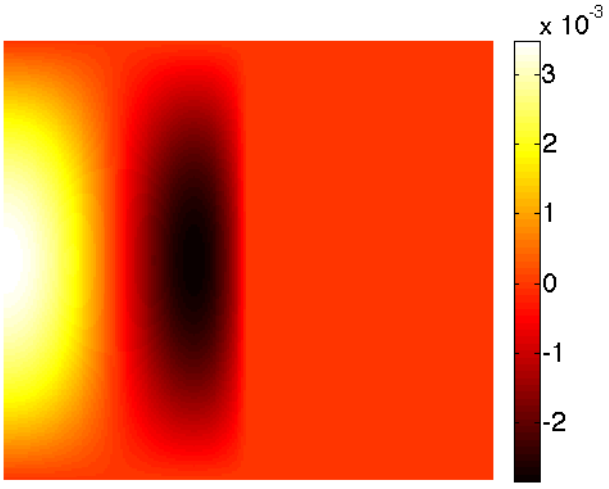

(b)

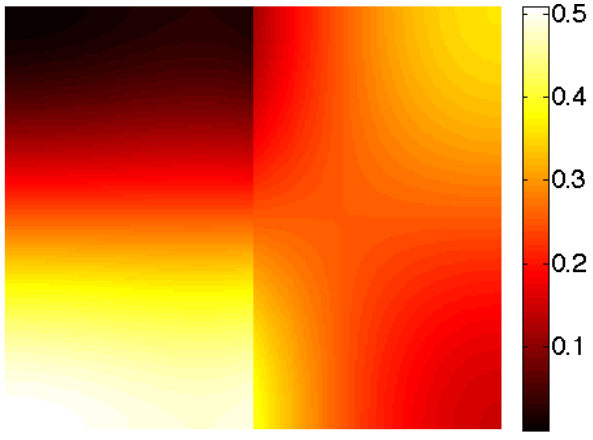

(c)

Fig. 3

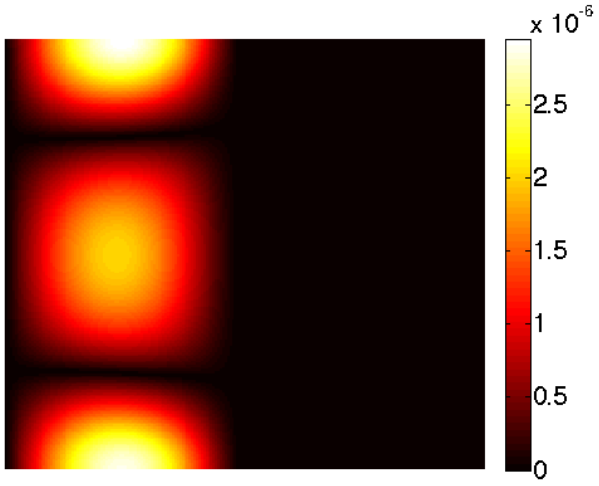

(a)

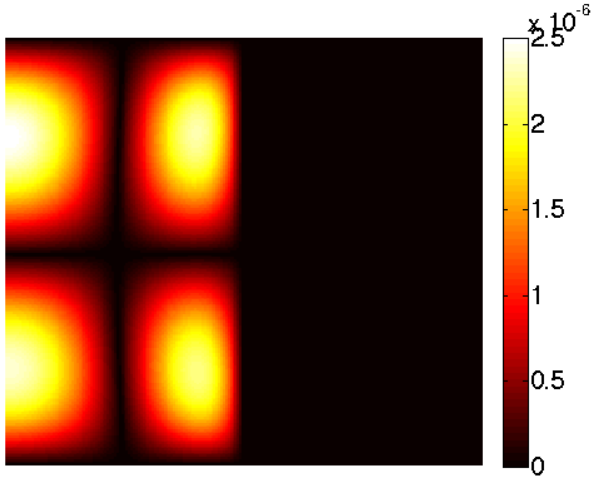

(b)

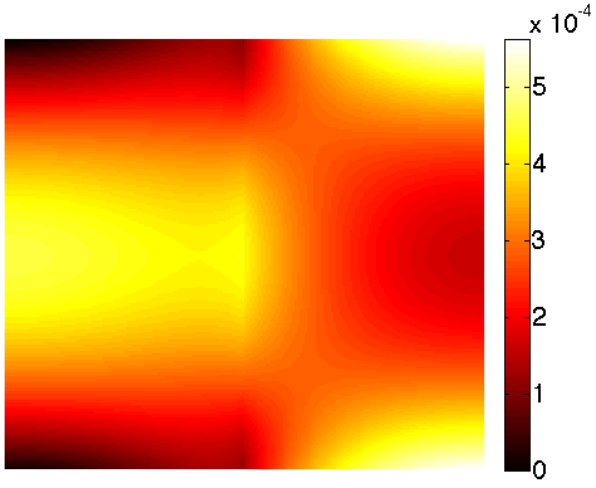

(c)

Fig. 4

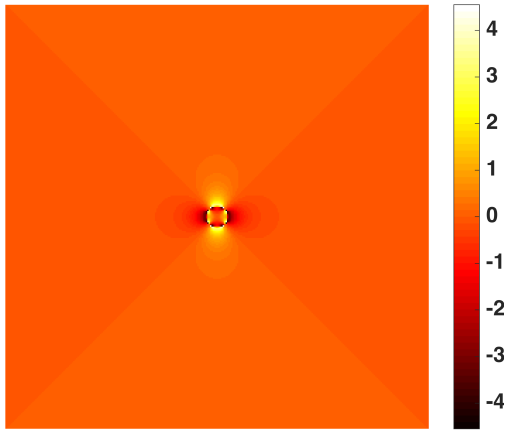

(a)

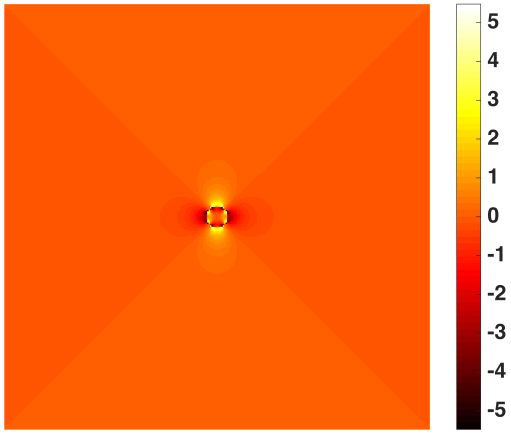

(b)

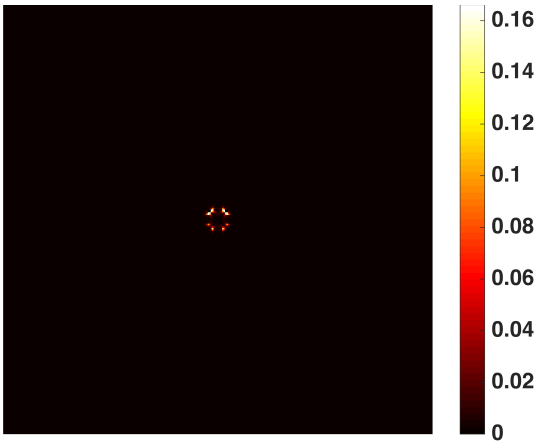

(c)

Fig. 5

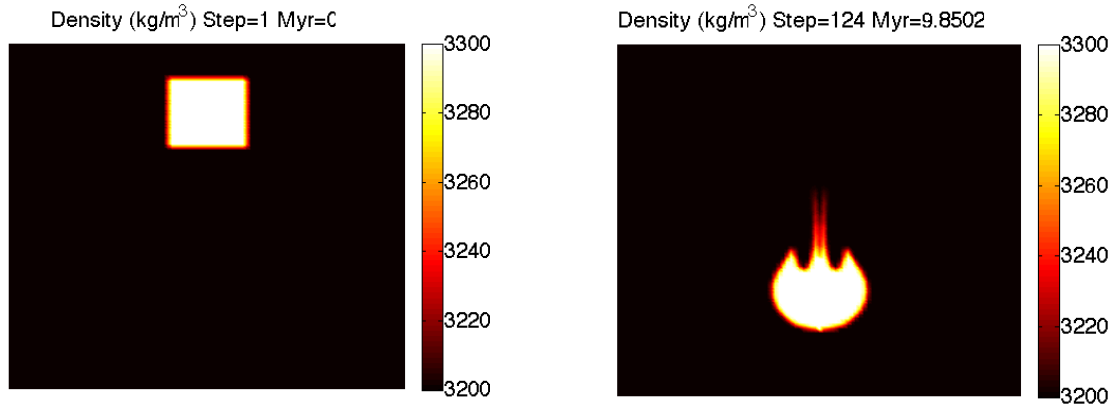
Density (kg/m3) Step=1 Myr=0
3300
3280
3260
3240
3220
3200

(a)

Density (kg/m3) Step=124 Myr=9.8502
3300
3280
3260
3240
3220
3200

(b)

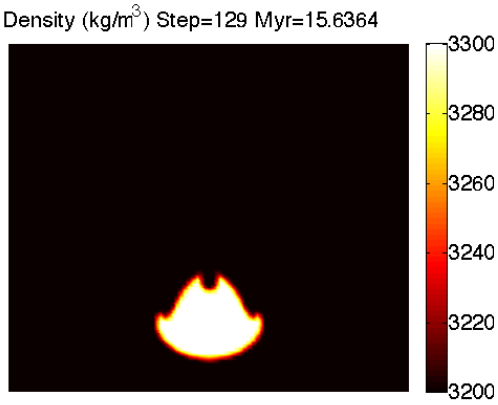
Density (kg/m3) Step=129 Myr=15.6364
3300
3280
3260
3240
3220
3200

(c)

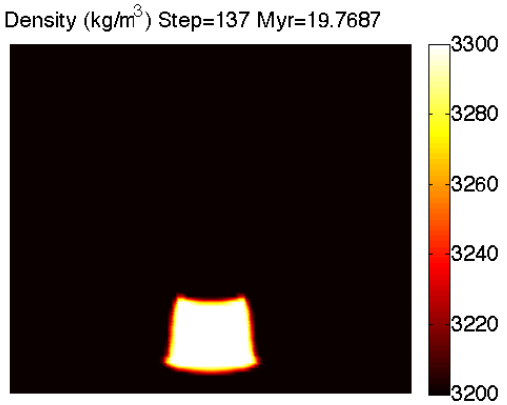
Density (kg/m3) Step=137 Myr=19.7687
3300
3280
3260
3240
3220
3200

(d)

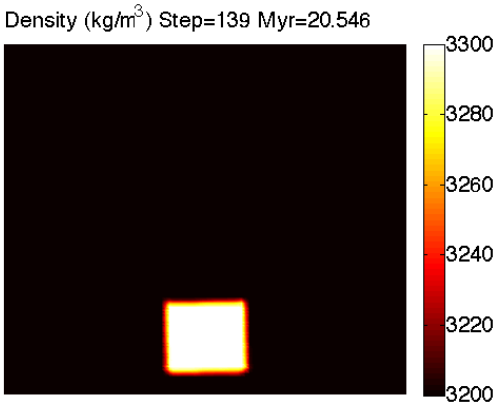
Density (kg/m3) Step=139 Myr=20.546
3300
3280
3260
3240
3220
3200

(e)

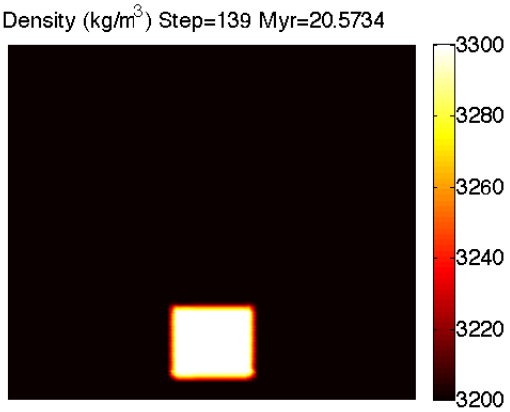
Density (kg/m3) Step=139 Myr=20.5734
3300
3280
3260
3240
3220
3200

(f)

Fig. 6

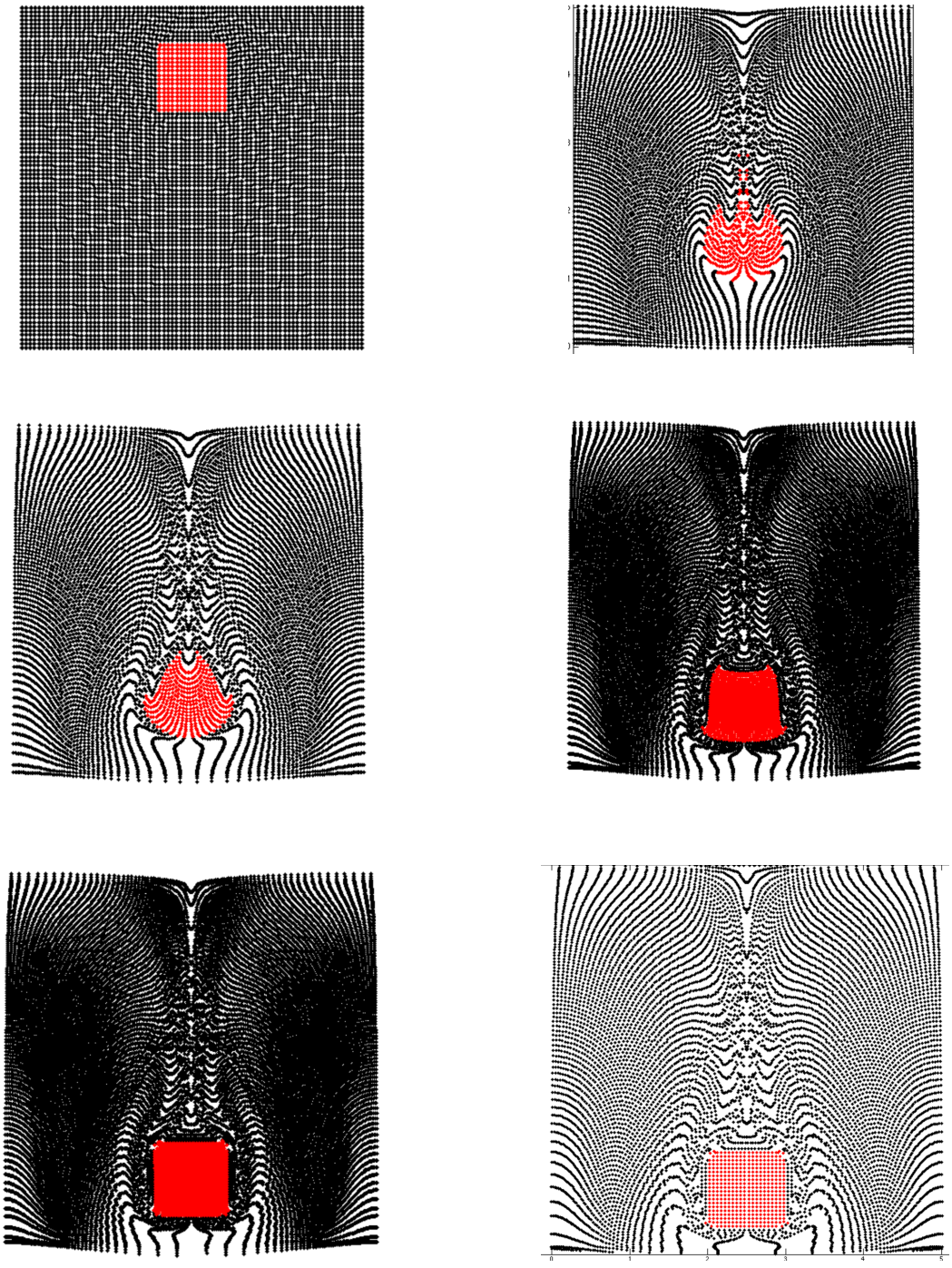

Fig. 7

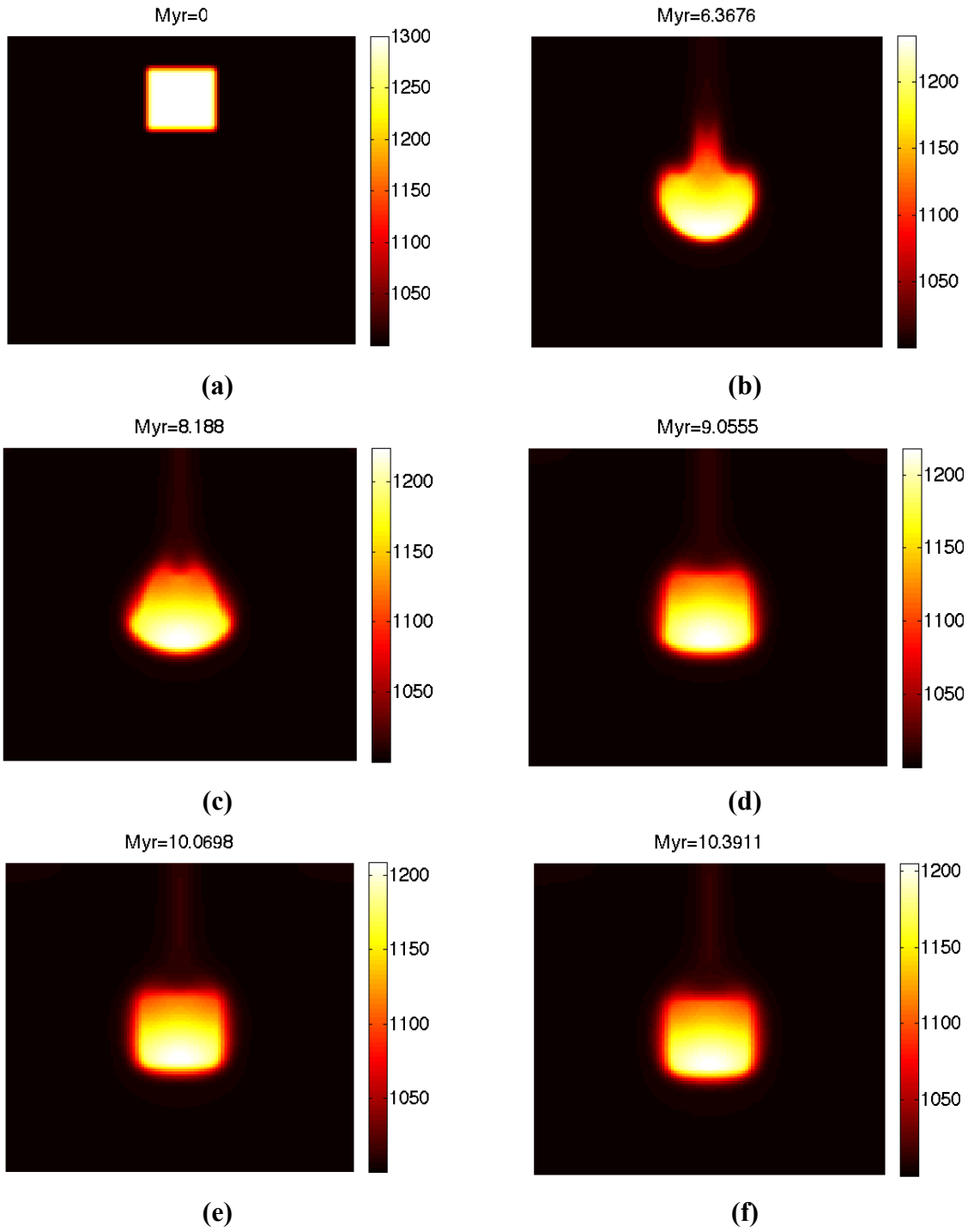
Myr=0
1300
1250
1200
1150
1100
1050
(a)
Myr=6.3676
1200
1150
1100
1050
(b)
Myr=8.188
1200
1150
1100
1050
(c)
Myr=9.0555
1200
1150
1100
1050
(d)
Myr=10.0698
1200
1150
1100
1050
(e)
Myr=10.3911
1200
1150
1100
1050
(f)

Fig. 8

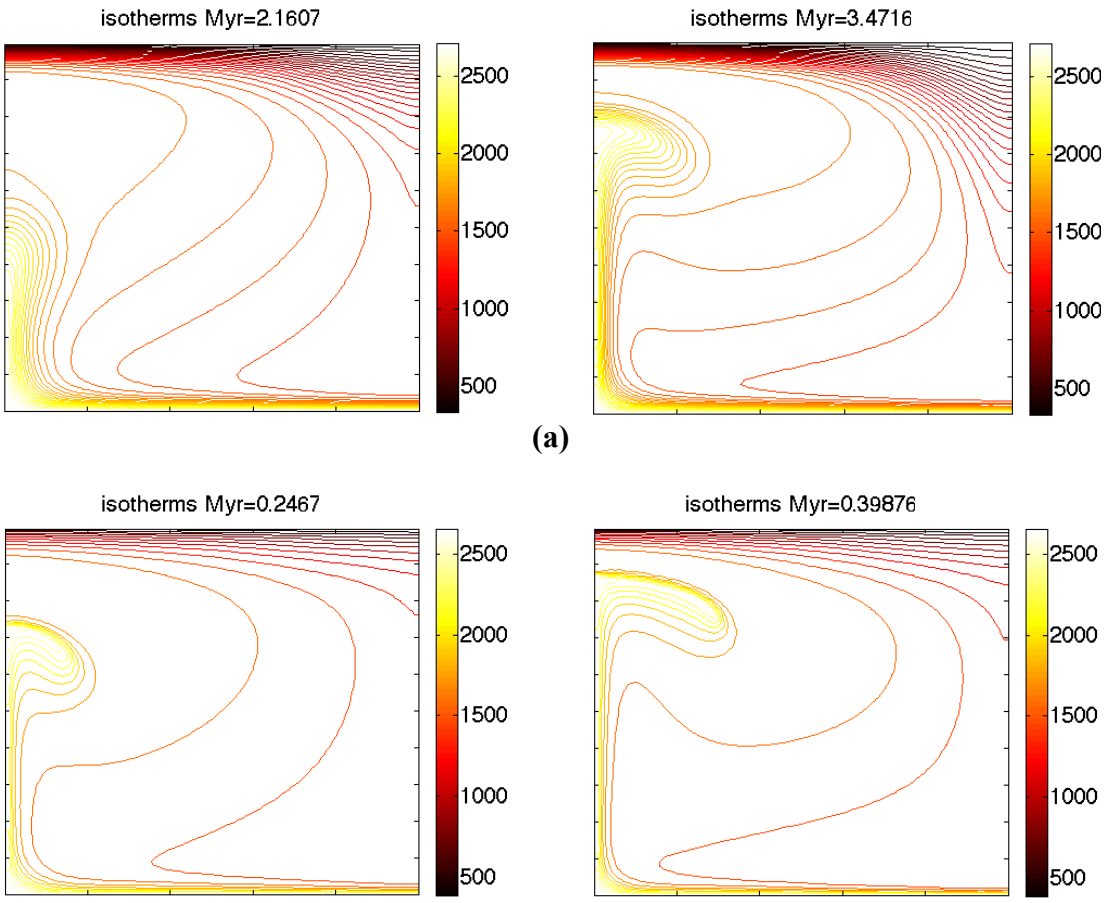
isotherms Myr=2.1607
2500
2000
1500
1000
500
isotherms Myr=3.4716
2500
2000
1500
1000
500
(a)
isotherms Myr=0.2467
2500
2000
1500
1000
500
isotherms Myr=0.39876
2500
2000
1500
1000
500
(b)

Fig. 9